IEEE Robotics and Automation Letters (RA-L) paper, presented at ICRA 2024, Yokohama, Japan. Cite as RA-L paper.

Torsion-Induced Compliant Joints and Its application to Flat-Foldable and Self-Assembling Robotic Arm

Dong-Wook Yang, Hyun-Su Park, Keon-Ik Jang, Jae-Hung Han*, and Dae-Young Lee*

***Abstract*— The joint design of origami-inspired robots is one of the most distinctive features that distinguishes them from conventional robots. A joint design using material's compliance enables origami robots to implement complex transformational movements in a lightweight and simple manner. However, utilizing the continuum bending mode of materials brings critical problems, including undesired movements and joint radius. This study introduces a solution to these problems through a torsion-based compliant joint (T-C joint) design, which utilizes the torsion deformation of materials. The potential of the T-C joint is demonstrated in a flat-foldable and self-assembling robotic arm, providing its applicability in environments with form-factor limitations and minimal human intervention. The robotic arm—comprising links, joints, and a gripper—can fold into a flat state, deploy with precision and minimal weight, and effectively manipulate target objects. This demonstration shows the real-world application of the proposed joint design.**

***Index Terms*—Compliant Joints and Mechanisms, Soft Robot Applications, Soft Robot Materials and Design, Origami-Inspired Mechanism, Self-Assembling Mechanism**

I. Introduction

An origami-inspired design approach that employs two-dimensional patterns of rigid facets and flexible hinges has emerged as a distinctive design tool in the field of robotics. This approach presents an alternative method for creating joint elements through a layer-based fabrication process, as opposed to traditional component assembly, significantly simplifying design, manufacturing, and assembly procedures. The resulting ease and expediency in fabrication not only facilitate access to previously challenging scales, such as micro-robots [1], [2] and medical robotics [3]–[5], but also enable dramatic, versatile shape transformations with uncomplicated mechanical configurations. These capabilities have been harnessed for diverse robotic applications, including robotic grippers [6]–[8], manipulators [9]–[11], mobile robots [12]–[14], and wearable robots [15], and space systems [16], [17].

In origami-inspired systems, joint design is a critical aspect, as its characteristics significantly influence the overall capabilities of the systems. In contrast to traditional joints that make hinge motion through the relative movement of discrete components, origami-based designs use a continuum body and rely on material deformation to achieve the same goal [18], [19]. While the origami approach offers structural simplicity, its applicability is restricted to specific applications due to inherent limitations tied to material properties. Typically, folding necessitates bending deformations within the material's strain boundaries, inevitably constraining the minimum folding radius. This folding radius, in turn, constrains the compression ratio, compromising the advantage of the origami structure. A more critical issue emerges when the excessive length of joint elements introduces undesired motion, substantially impairing the structure's rigidity and stability.

In previous studies, it was confirmed that utilizing both bending and torsion properties together through drilling rectangular holes in specific locations results in a relatively small folding radius compared to using only bending property [20], [21]. Additionally, in other study, elliptical holes were regularly drilled to utilize the torsion property for folding [22]. Manen et al. use a single slit at center for stretching [23], while Eda et al. use open holes [24]. In most cases, relatively large holes were employed to create crosswise arrangement patterns, stacking them on top of each other to achieve significant large curvature [23]–[26]. Previous methods have induced torsion by creating relatively large holes, which resulted in significant bending effects in the surrounding area and required larger joint sizes. Additionally, further analysis of the elastic range is necessary. The key concept here is to focus on maximizing the torsion property of materials to reduce the folding radius and minimize the size of the joint by patterning with narrow slits.

In this study, we present a design framework for a Torsion-Induced Compliant Joint (T-C joint) that fully exploits the material's elastic region to enable a simple and efficient design. We constructed an analytical model to provide the theoretical ground on the proposed design and identified essential design parameters that determine the characteristics of the joint to ensure the adaptability of this design to a broad range of applications. Additionally, we cross-validated the trends associated with these parameters through the analytical model, finite element analysis (FEA), and extensive experiments. The primary advantages of the proposed joint design are as follows

Manuscript received June 2, 2023; Revised August 26, 2023; Accepted September 18, 2023. This paper was recommended for publication by Editor Young-Lae Park upon evaluation of the Associate Editor and Reviewers' comments. This work was supported by the National Research Foundation of Korea (NRF) grant funded by Ministry of Science and ICT (No. 2022R1C1C1003718, No. 2022M1A3C2069728, No. NRF-2021R1A2C2004563) and the BK21 FOUR Program funded by Ministry of Education. (*Corresponding author: Jae-Hung Han and Dae-Young Lee*).

D.-W. Yang, H.-S. Park, K.-I. Jang, J.-H. Han and D.-Y. Lee is with the Department of Aerospace Engineering, Korea Advanced Institute of Science and Technology (KAIST), Daejeon 34141, Republic of Korea (e-mail: ydw011@kaist.ac.kr; hyunsu1107@kaist.ac.kr; kijang@kaist.ac.kr; jaehunghan@kaist.ac.kr; ae_dylee@kaist.ac.kr). Digital Object Identifier (DOI): see top of this page.

IEEE Robotics and Automation Letters (RA-L) paper, presented at ICRA 2024, Yokohama, Japan. Cite as RA-L paper.

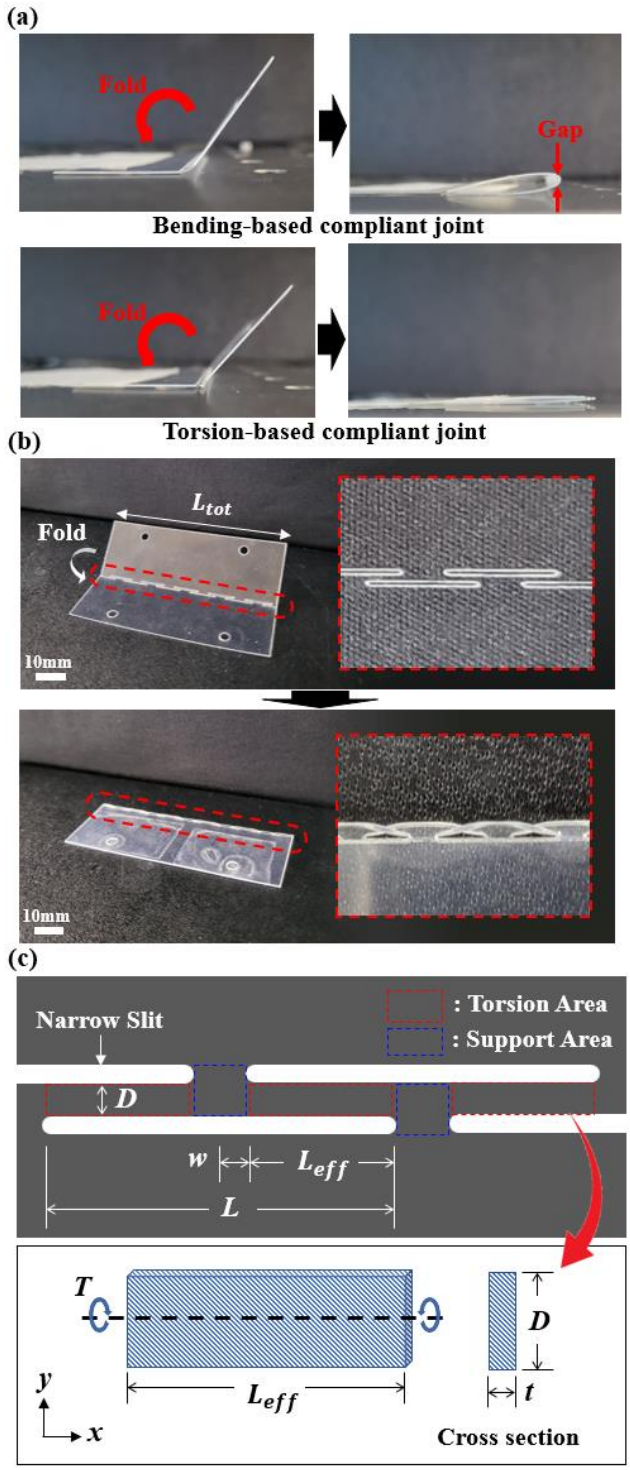

Fig. 1. (a) Comparison between two joints. (b) T-C joint folding. (c) Joint parameters.

(movie S1; See the supplementary movies):

(1) Ultra-thin profile: A single sheet of material can function as a revolute joint with a zero bending radius, enabling the achievement of a high compression ratio (almost no internal gap when folded).

(2) Ideal joint motion: Despite relying on material deformation, the design allows for a folding angle of up to 180 degrees without inducing plastic deformation. More importantly, in contrast to compliant joints utilizing bending modes, the torsion-based joint features a singular, well-defined rotational axis that remains fixed irrespective of the joint angle.

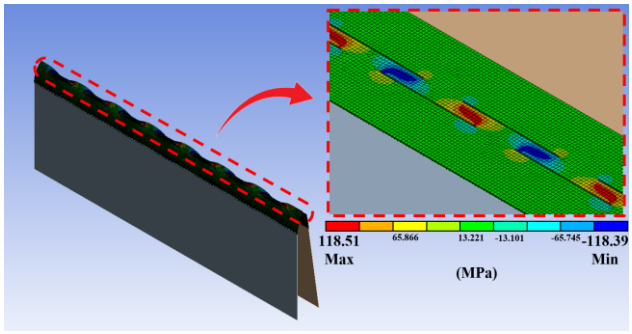

Fig. 2. T-C joint FEA modeling

(3) Inherent joint stiffness: Self-deploying or assembling systems typically necessitate multiple joints with sufficient stiffness to enable structure construction while minimizing the number of actuators and ensuring stable deployment. Through parameter adjustments derived from the analytical model, the T-C joint can achieve the desired stiffness without the need for additional spring components, allowing the implementation of intricate deployment sequences while maintaining structural simplicity and lightness.

(4) Versatility in material choice: The proposed model enables the tailoring of the joint design parameters to prevent plastic deformation considering strain limits and material thicknesses. Consequently, the T-C joints can be fabricated from a diverse selection of sheet materials, including engineering plastics, steel, and composite materials.

To verify the potential of the proposed design, we showcased a flat-foldable self-assembling robotic arm based on T-C joints that deploys without additional actuators. Self-assembling robots are promising in extreme environments such as the human body or outer space, where form factors are constrained, and human intervention is limited [12], [27]. A primary challenge in actualizing self-assembling robots lies in the implementation of intricate folding sequences for the assembly procedure. Passive folding joints have not been typically employed for self-assembling robots due to the complexities in embedding elastic elements, as well as the challenges associated with attaining substantial folding angles.

The developed robotic arm is composed of links, joints, and a gripper, where in each component is capable of folding into a flat configuration. The link component can be assembled into a rigid bar shape through sequential perpendicular folds. The joint component self-locks in the flat-folded state, transitioning into the free rotation state upon deployment. The gripper component can be assembled into a special configuration that allows adaptive object grasping with a single actuator. The deployable parts of this robotic arm have been confirmed to deploy from 3mm (25mm for including bolts and nuts) to 445mm with a weight of 121.1g, and demonstrates successful manipulation of target objects.

IEEE Robotics and Automation Letters (RA-L) paper, presented at ICRA 2024, Yokohama, Japan. Cite as RA-L paper.

II. TORSION-INDUCED COMPLIANT JOINT

A. Design and Folding Mechanism

T-C joint incorporates cutting narrow lines arranged in a staggered slit pattern to induce torsion of the material during folding (Fig. 1(b)). During folding, shear stress is concentrated in a specific area as shown in Fig. 1(b). To simplify the analytical model of the T-C joint, the joint can be divided into the torsion area, the red area in Fig. 1(c), where torsion occurs, and the support area, the blue area in Fig. 1(c), which transmits the moment. Due to the use of a narrow slit to form the pattern, the support area's length becomes minimized, providing sufficient bending stiffness. We also analyzed the behavior of the given structure using finite element analysis (FEA) (Fig. 2). The FEA model was constructed using the ANSYS software. The area surrounding the pattern in the CAD model, matching the experimental specimen, was meshed with a size of 0.2mm over an 8mm region. Large deflection and weak spring modes were enabled, and motion was simulated using remote displacement. Fig. 2 shows results that match well with our previous assumptions. In summary, the T-C Joint implements folding as a moment is applied, and the moment is transmitted through the support area to the torsion area, resulting in twisting in the designated area.

B. Modeling & Analysis

The design parameters of the T-C joint is illustrated in Fig. 1(c), which include the length of the constituent line (L), the half-length of the support area (w), and the distance between two lines on the opposite side (D). Moreover, the effective length of the torsion area (L_{eff}) and the number of areas (N_{eff}) are included. Leff can be expressed by L and w.

$$L_{eff} = \frac{L}{2} - w \tag{1}$$

The torsion area of the joint can be modeled as a thin rectangular beam. Also, for simplification, we assumed that joint can be folded without bending in support area. When a torque T is applied to a rectangular beam composed of a material with shear modulus G and thickness t, the resulting twist angle θ can be described by the following equation derived from [28], [29].

$$\theta = 3TL_{eff}/DGt^3\{1 - 0.63\frac{t}{D}\left(1 - \frac{1}{12}\frac{t^4}{D^4}\right)\} \tag{2}$$

In this case, the torsional stiffness (K_{eff}) of a single torsion area can be determined by the equation, $T = K_{eff}\theta$, where T is the torque applied and θ is the resulting twist angle. The expression for K_{eff} can be given by the following equation:

$$K_{eff} = \frac{T}{\theta} = \left\{\frac{1}{3}\frac{D}{t} - 0.21\left(1 - \frac{1}{12}\frac{t^4}{D^4}\right)\right\}\frac{Gt^4}{L_{eff}} \tag{3}$$

Considering that the T-C joint comprises N_{eff} torsion areas, the overall torsional stiffness K can be expressed as follows:

$$K = N_{eff}K_{eff} \tag{4}$$

The parameters t, D, and L_{eff}, which directly impact the overall torsional stiffness, will be categorized as critical parameters. (Note that G is material-dependent variables.)

When a torque T is applied to the T-C joint, as illustrated in Fig. 1(c), the maximum shear stress in the x-y axis acting on a single torsion area can be expressed as $\tau_{smax,xy}$, as given by the following equation (5) [29], where k_1/k_2 is a non-dimensional constant determined by D/t [28], [29].

$$\tau_{smax,xy} = \frac{T}{k_1 Dt^2} \tag{5}$$

Deformation θ can be expressed by using k_1 as follows.

$$\theta = \frac{TL_{eff}}{k_1 Dt^3 G} \tag{6}$$

By modifying the above equation, expression for T is obtained. Substituting T into the shear stress equation and utilizing the relationship between stress and strain yields the shear strain equation.

$$\tau_{smax,xy} = \frac{T}{k_1 Dt^2} = \frac{k_1}{k_2}\frac{t}{L_{eff}}G\theta = G\gamma_{xy} \tag{7}$$

$$\therefore \gamma_{xy} = \frac{k_1}{k_2}\frac{t}{L_{eff}}\theta \tag{8}$$

The approximate value of the principal strain applied to the torsion area can be obtained from equation (9), and it must be less than the yield strain to ensure the joint operates within the elastic range.

$$\text{Principal strain}\left(\varepsilon_x, \varepsilon_y \approx 0\right) = \frac{1}{2}\gamma_{xy} = \frac{1}{2}\frac{k_1}{k_2}\frac{t}{L_{eff}}\theta \tag{9}$$

The equation can be further modified to obtain a condition for L_{eff} as follows.

$$\frac{1}{2}\frac{k_1}{k_2}\frac{t}{(\text{yield strain})}\theta < L_{eff} \tag{10}$$

The boundary condition dictates that the combined length of the torsion area, should not exceed the total length of the joint.

$$L_{eff}\, N_{eff} < L_{tot} \tag{11}$$

The minimum value of L_{eff} required to achieve the desired aspect ratio and folding angle of the torsion area can be calculated using the condition of L_{eff}. Similarly, the maximum value of N_{eff} can be determined when L_{eff} is at its minimum value, as per the boundary condition. The maximum value of torsional stiffness under the desired conditions can be achieved using a mathematical model, provided that the minimum value of L_{eff} and the maximum value of N_{eff} are available.

The identical modeling and analysis were considered for the bending joints to compare folding performance with T-C joints. This type of joint is referred to as the "Bending compliant joint." The torsional stiffness of the Bending Joint can be determined using Equation (12) from [20], assuming that it behaves like a pure beam bending case. The maximum strain in the y-direction at the desired joint width, D, and deformation angle, θ, can be approximated by the ratio of the distance between the neutral surface and the outermost surface and the radius of curvature of the neutral surface from [29].

$$K_{bending} = \frac{EL_{tot}t^3}{12D} \tag{12}$$

IEEE Robotics and Automation Letters (RA-L) paper, presented at ICRA 2024, Yokohama, Japan. Cite as RA-L paper.

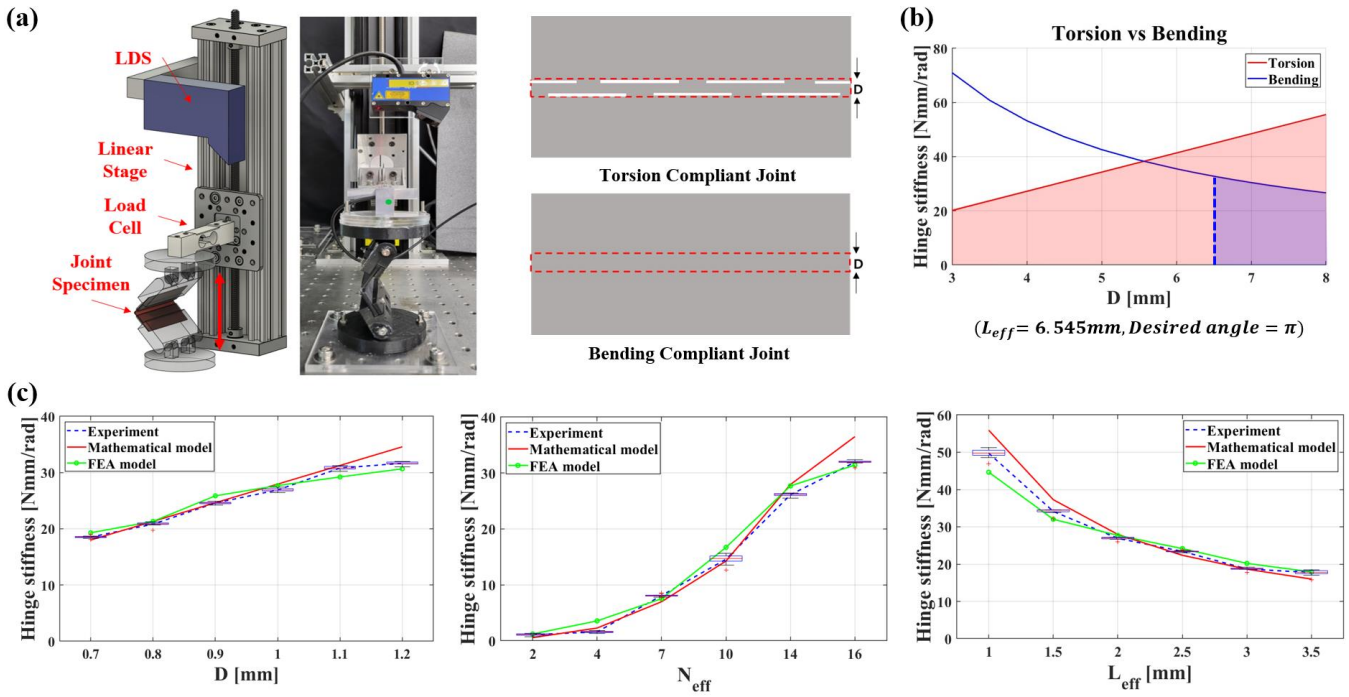

Fig. 3. Torsional Stiffness Experiments. (a) A test setup and joint schematics. (b) A mathematical comparison between T-C joints and bending compliant joints. (c) The results of the torsional stiffness test according to experiment parameters.

$$\varepsilon_{y,max} = \frac{t/2}{D/\theta} = \frac{t\theta}{2D} \tag{13}$$

The principle strain applied to the bending beam can be estimated using Equation (14), which must be less than the yield strain to ensure that the joint functions within the elastic range.

$$\text{Principal strain}\left(\varepsilon_x, \gamma_{xy} \approx 0\right) = \varepsilon_{y,max} = \frac{t\theta}{2D} < (\text{yield strain}) \tag{14}$$

By modifying the above equation, a condition of D is obtained as follows:

$$\frac{t}{2}\frac{\theta}{(yield\ strain)} < D \tag{10}$$

The minimum value of D can be obtained through this condition, and the maximum value of the torsional stiffness for the joint operating under desired conditions can also be obtained.

As previously mentioned, the width dimension of the compliant joint is critical as it creates undesired motion. Therefore, it is necessary to verify whether the joint has sufficient torsional stiffness even when used with a various width. Fig. 3(b) shows the maximum torsional stiffness values for the bending compliant joint and the T-C joint according to the width dimension (set yield strain=0.06, t=0.25mm, and θ=π).

The important point to note is that the T-C joint utilizes torsion, and hence it allows for a wide range of D values while maintaining strain within the elastic range by adjusting L_{eff}. However, the width of the bending compliant joint, denoted as 'D' in Fig. 3(a), is limited due to the restriction of the elastic range required to fold it at the desired angle.

Therefore, we were able to confirm that the T-C joint offers the advantage of being used freely in a wider range. (i.e., the available area of the T-C joint, shaded in red, is wider than that of the bending joint, shaded in blue.) Additionally, since the T-C joint has various parameters to set, the lack of stiffness can be fulfilled by adjusting the parameters or using suitable materials. One important thing to note is if D exceeds twice the thickness of the material, it can create an out-of-plane protrusion in the folded configuration, which can make it vulnerable to external forces such as compression. This needs to be considered when setting design parameters. The conclusion was reached that even though the newly designed T-C joint has a smaller width than the normal bending compliant joint, it performs better in angular folding.

C. Experimental validation

An experiment was conducted to measure and compare the torsional stiffness of the physical model in order to verify the models obtained in the previous section. The compliant joint specimens used in the experiment was produced using PET (Polyethylene terephthalate) with a thickness of t = 0.25 mm, as shown in Fig. 1(b). The compliant joint specimens had a width of 48 mm and a length of 70 mm and contained the T-C joint's crease line in the center.

TABLE I
EXPERIMENT PARAMETERS

$D(mm)$	0.7	0.8	0.9	1.0*	1.1	1.2
N_{eff}	2	4	7	10	14*	16
$L_{eff}(mm)$	1	1.5	2*	2.5	3	3.5

IEEE Robotics and Automation Letters (RA-L) paper, presented at ICRA 2024, Yokohama, Japan. Cite as RA-L paper.

In order to analyze the characteristics of T-C joints, three experiment parameters were defined: the width of torsion area, D, the total number of the torsion area, N_{eff}, and the length of torsion area, L_{eff}. Reference experiment parameters were set as [D, L_{eff}, N_{eff}] = [1*mm, 2*mm, 14*]. The experiment was conducted by varying one variable for each parameter, as indicated in Table I.

The customized experimental device measures the force using a load cell and the displacement using an LDS, as depicted in Fig. 3(a)[22]. The torsional stiffness value, K, can be determined based on the equation '$T=K\theta$' since force can be converted to torque T and displacement to deformation θ, and the size of the compliant joint specimen is known.

The experiment was divided into two stages. In the first stage, a cycle test, which involves a repetitive loading and unloading process, was performed 20 times or more to obtain a constant torsional stiffness value from the specimen. In the second stage, actual torsional stiffness was measured by operating the linear stage from the initial 135 to 90 degrees folding angle and obtaining data by measuring 10 times per specimen. The torsional stiffness value was calculated based on the average of the actual data obtained.

The PET used in the experiment was 0.25 mm thick, and the shear modulus G was 0.89 GPa. The stiffness value that was calculated by the mathematical model is represented by a red line, the data from FEA model is represented by a green line, and the actual value measured by the experiment is shown by a blue dotted line using a box plot in Fig. 3(c). The box plots summarizing the results for the three experiment parameters are shown in Fig. 3(c).

The discrepancies between the analytical prediction and the measured value might arise from the assumption regarding the bending of the support area in the analytical model. Additionally, while the assumption of linearity in material properties could introduce inaccuracies, the impact is likely minimal given that we operated within the elastic range of the material. As the rotation angle of the joint increases, the potential for errors due to these assumptions might also intensify.

III. Manipulator Implementation

A. Flat-Foldable and Self-Assembling Robotic Arm

The conceptual design for a flat-foldable and self-assembling robotic arm was developed by taking advantage of the concise pattern and folding-optimized characteristics of the T-C Joint. Previous deployable robotic arms either made only the link part deployable [30] or had no joints at all [31]. However, in this study, the tendon-driven method was selected to replace big servo motors and apply foldable joints [32]. Additionally, joints were maintained by designing them with an origami structure for folding. The gripper also adopted an origami structure that can be folded. The link was designed to be deployable and rigid by combining the sarrus linkage with wings for shape retention.

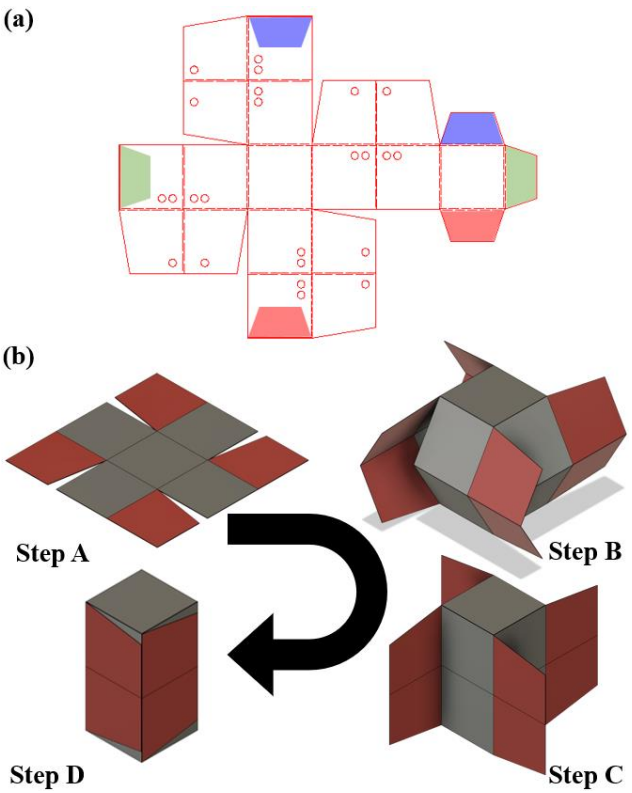

Fig. 4. A self-assembling sarrus linkage cube. (a) A planar figure. (b) An assembling mechanism.

B. Robotic Arm Link: Self-Assembling Sarrus linkage Cube

By utilizing the 4-sided sarrus linkage, it is possible to transform from a flat state to a cube through four steps, as shown in Fig. 4(a), (b). Hence, the T-C joint, optimized for folding, was employed in the folding section of the sarrus linkage to enable circular motion. Furthermore, the T-C joint possesses inherent stiffness, allowing it to self-assemble into a cube from a plane without requiring a separate actuator. The wing structure, red sections in Fig. 4(b), folds perpendicular to the direction of cube deployment. It provides additional rigidity to the cube by fixing the movement in the direction of deployment.

In the sarrus linkage cube, certain areas require 180-degrees of folding while others require 90-degrees of folding. Consequently, the joint parameters were optimized based on the necessary folding angle and crease line size, utilizing the L_{eff} condition and boundary conditions obtained through elastic strain analysis.

A $60\text{mm} \times 60\text{mm} \times 120\text{mm}$ cube was fabricated as the robotic arm's link, using a PET material. In each joint part, the initial state was established through heat forming process. An additional thin neodymium magnet was attached to enable the four wings to be fixed after deployment. The cube can be compressed to 0.5 mm, which corresponds to the thickness of two PET sheets. Upon deployment, it extends to a height of 120 mm, approximately 240 times its initial height, as illustrated in movie S2.

IEEE Robotics and Automation Letters (RA-L) paper, presented at ICRA 2024, Yokohama, Japan. Cite as RA-L paper.

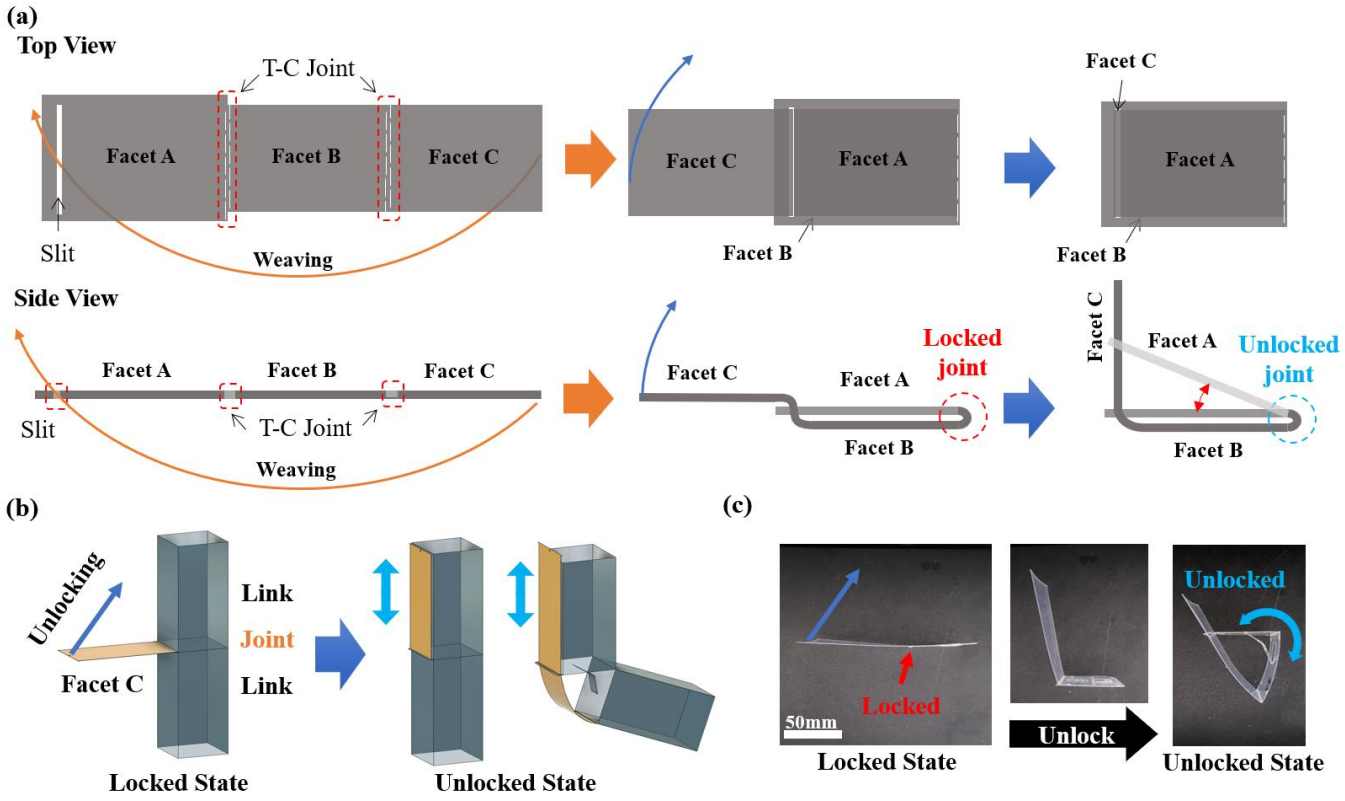

Fig. 5. A self-locking joint. (a) A locking mechanism. (b) A working process of the joint in the robotic arm. (c) A real model.

C. Robotic Arm Self-Locking Joint Design

Unlike conventional robotic arms, which are driven by motors installed in each joint, we consolidate all motors into a single driving unit for tendon-driven operation. By extracting the driving unit from the joint, the joint can be folded while the shaft rotation function is still maintained. This origami-inspired joint achieves excellent folding performance by utilizing T-C joints, as depicted in Fig. 5(a). However, when the joint is attached, it causes an undesired rotation during the deployment of the robotic arm, which interferes with fully deployment. Therefore, this joint is designed to be self-locking during deployment to prevent unnecessary movement. This joint, as shown in Fig. 5(a), is fixed by weaving one end into the opposite slit, so it does not move even when the robot arm is deployed. Lifting the longer end allows it to pass through the slit freely, enabling it to rotate like a regular joint. In the robotic arm system, it will be unlocked by a tendon pulling and will function as normal joints, as shown in Fig. 5(b), (c).

D. Robotic Arm Origami Gripper Design

There are two ways to grasp an object: pinching mode is where the gripper grasps an object by tightly pinching it at multiple points, while enveloping mode is where the gripper surrounds and holds an object using its arms, making it useful for larger or softer objects [33]. Typically, multiple actuators are required to construct a gripper capable of performing these two modes. However, connecting multiple actuators using wires can increase complexity due to tendon-driven limitations. Therefore, this gripper, fabricated from flexible materials, adapts to the shape of an object by changing the grabbing method when the wire is pulled. If the wire is not pulled, the initial shape is fixed through heat processing, allowing the gripper to return to its original position. By this principle, this gripper can be driven by a single wire. Fig. 6(a) shows the

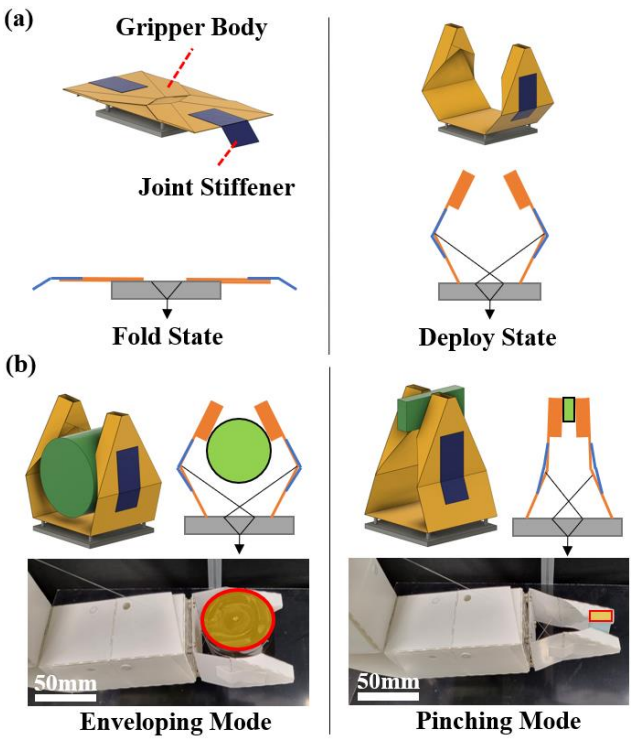

Fig. 6. An origami gripper. (a) A deployment mechanism. (b) A grasping mechanism with a real model.

IEEE Robotics and Automation Letters (RA-L) paper, presented at ICRA 2024, Yokohama, Japan. Cite as RA-L paper.

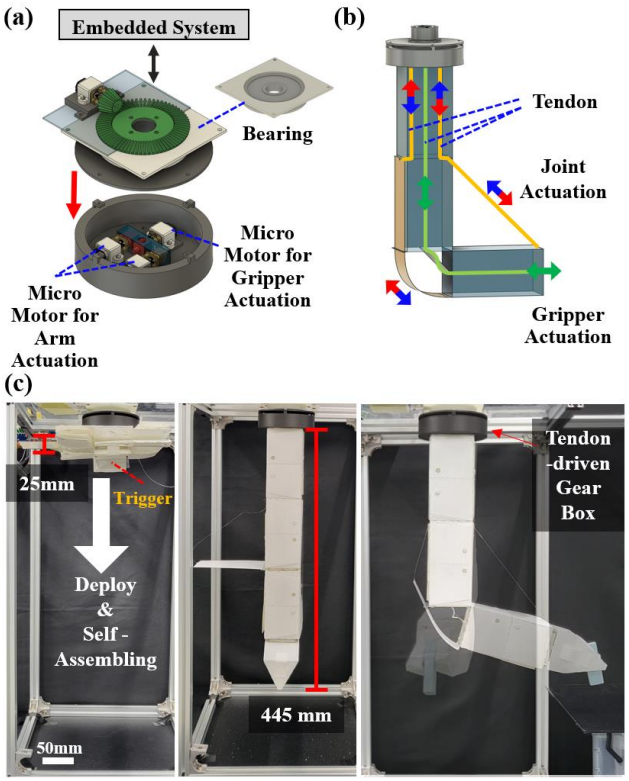

Fig. 7. A flat-foldable and self-assembling robotic arm. (a) The components of tendon-driven gear box. (b) The wire connections of the robotic arm. (c) A demonstration of the robotic arm.

model of the newly designed origami-inspired gripper, which is divided into a gripper body, orange part, whose angle changes according to the object's shape, and a joint stiffener, blue part, responsible for transmitting force to end and preventing the gripper's end from spreading apart. Because of T-C joints in the structure, it can be self-deployed as shown in Fig. 6(a). In enveloping mode, shown in Fig. 6(b), the blue part aligns the orange tongs' shape to match the object's shape, enabling us to surround and pick up the object. By pulling the wire, it transitions into a pinching mode, allowing it to tightly pinch objects. In pinching mode, shown in Fig. 6(b), the blue part applies greater force to enable pinching while keeping the gripper's end from spreading apart, and the tip of the tongs aligns with the object's shape, enabling the object to be picked up.

E. Performance

The proposed robotic arm can be folded flat using the origami principle, including the link, joint, and gripper. Angled objects can be picked up with a specially designed gripper, or round objects can be picked up, as shown in Fig. 6(c). Furthermore, it was verified that the self-assembling sarrus linkage cube, weighing only 25g, can endure up to 2000g, which is roughly 80 times its weight without an actuator input.

In object manipulation, the tendon-driven gearbox, which is connected to the embedded system, uses 2 high-gear ratio micro metal motors for arm actuation, 1 motor for rotation, and 1 motor for gripper actuation (Fig. 7(a)). As shown in Fig. 7(b),

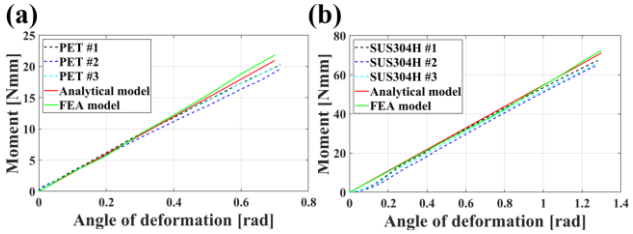

Fig. 8. (a) PET moment graph (b) SUS304H moment graph

the two orange-colored tendons are used to move the arm up and down, and they move in the opposite direction to create the tension, preventing the arm from twisting. Another green-colored tendon is used for opening and closing the gripper. All flat-foldable and self-assembling parts of this robotic arm have been confirmed to deploy from 3mm (25mm for including bolts and nuts) to 445mm with a weight of 121.1g and demonstrate successful manipulation of target objects (<350g) (Fig. 7(c) and movie S3).

IV. Discussion

In this study, we developed a torsion-based compliant joint, apt for folding movements, utilizing a simple pattern and performed parametric analyses. We confirmed that the T-C joint can enable folding motion within a small radius without exceeding the material's elastic range, a noticeable improvement over common bending compliant joint. Moreover, it is shown that desired stiffness can be achieved by adjusting the parameters via the torsional stiffness equation derived from the analytical model. We conducted experiments by introducing a T-C joint pattern into a 0.1mm thick SUS304H specimen. As illustrated in Fig. 8(a) and (b), we confirmed that the FEA model and analytical model adequately follows the overall behavior of the actual model. We posit that there exists substantial potential for the application of this methodology with materials beyond PET. As inaccurate and uncontrollable movements have been significant limitations of compliant joints that restrict the widespread use of origami-inspired designs, the proposed solution holds substantial potential in mitigating this issue.

Space robotics, particularly deployable or self-assembling variants, are a primary target of our efforts. In space, system volume and simplicity become crucial considerations. The proposed design, while being low-profile and composed of single-material, can perform the role of an elastic joint, simplifying complex deployment sequences required for self-assembly. Another essential feature we wish to highlight is the versatility of this design, applicable to a wide range of materials. Sophisticated design parameters enable the design of joint movements within the elastic range of any materials, facilitating the usage of space-suitable materials like steels or composites. We believe this novel joint design could play a critical role in expanding the application range of origami-inspired robotics including space application.

V. Acknowledgment

We would like to acknowledge the technical support from ANSYS Korea.

IEEE Robotics and Automation Letters (RA-L) paper, presented at ICRA 2024, Yokohama, Japan. Cite as RA-L paper.

REFERENCES

[1] M. Z. Miskin *et al.*, "Electronically integrated, mass-manufactured, microscopic robots," *Nature*, vol. 584, no. 7822, pp. 557–561, Aug. 2020.

[2] Y. Zhu *et al.*, "Elastically and Plastically Foldable Electrothermal Micro-Origami for Controllable and Rapid Shape Morphing," *Adv. Funct. Mater.*, vol. 30, no. 40, p. 2003741, Oct. 2020.

[3] H. Suzuki and R. J. Wood, "Origami-inspired miniature manipulator for teleoperated microsurgery," *Nat. Mach. Intelligence.*, vol. 2, no. 8, pp. 437–446, Jul. 2020.

[4] A. Ghosh *et al.*, "Stimuli-Responsive Soft Untethered Grippers for Drug Delivery and Robotic Surgery," *Front. Mech. Eng.*, vol. 3, Jul. 2017.

[5] B. Sargent *et al.*, "An Origami-Based Medical Support System to Mitigate Flexible Shaft Buckling," *J. Mech. Robot.*, vol. 12, no. 4, Aug. 2020.

[6] A. Firouzeh and J. Paik, "Grasp Mode and Compliance Control of an Underactuated Origami Gripper Using Adjustable Stiffness Joints," *IEEE/ASME Trans. Mechatronics*, vol. 22, no. 5, pp. 2165–2173, Oct. 2017.

[7] J. A. Faber, A. F. Arrieta, and A. R. Studart, "Bioinspired spring origami," *Science*, vol. 359, no. 6382, pp. 1386–1391, Mar. 2018.

[8] S. Li *et al.*, "A Vacuum-driven Origami 'Magic-ball' Soft Gripper," *2019 Int. Conf. Robot. Automat. (ICRA)*, Montreal, May 2019, pp. 7401–7408.

[9] M. Boyvat, J.-S. Koh, and R. J. Wood, "Addressable wireless actuation for multijoint folding robots and devices," *Sci. Robot.*, vol. 2, no. 8, Jul. 2017.

[10] H. Matsuo, H. H. Asada, and Y. Takeda, "Design of a Novel Mutliple-DOF Extendable Arm With Rigid Components Inspired by a Deployable Origami Structure," *IEEE Robot. Automat. Lett.*, vol. 5, no. 2, pp. 2730–2737, Apr. 2020.

[11] M. Park *et al.*, "Deployable Soft Origami Modular Robotic Arm With Variable Stiffness Using Facet Buckling," *IEEE Robot. Automat. Lett.*, vol. 8, no. 2, pp. 864–871, Feb. 2023.

[12] S. Felton, M. Tolley, E. Demaine, D. Rus, and R. Wood, "A method for building self-folding machines," *Science*, vol. 345, no. 6197, pp. 644–646, Aug. 2014.

[13] D.-Y. Lee *et al.*, "Origami Wheel Transformer: A Variable-Diameter Wheel Drive Robot Using an Origami Structure," *Soft Robot.*, vol. 4, no. 2, pp. 163–180, Jun. 2017.

[14] D.-Y. Lee, J.-K. Kim, C.-Y. Sohn, J.-M. Heo, and K.-J. Cho, "High–load capacity origami transformable wheel," *Sci. Robot.*, vol. 6, no. 53, Apr. 2021.

[15] S. Seo *et al.*, "Origami-Structured Actuating Modules for Upper Limb Support," *IEEE Robot. Automat. Lett.*, vol. 6, no. 3, pp. 5239–5246, Jul. 2021.

[16] L. Wilson, S. Pellegrino, and R. Danner, "Origami Sunshield Concepts for Space Telescopes," in *54th AIAA/ASME/ASCE/AHS/ASC Structures, Structural Dynamics, and Materials Conf.*, Reston, Apr. 2013.

[17] M. Arya *et al.*, "Origami-Inspired Optical Shield for a Starshade Inner Disk Testbed: Design, Fabrication, and Analysis," in *AIAA Scitech 2021 Forum*, Reston, Jan. 2021.

[18] S.-R. Kim, D.-Y. Lee, S.-J. Ahn, J.-S. Koh, and K.-J. Cho, "Morphing Origami Block for Lightweight Reconfigurable System," *IEEE Trans. Robot.*, vol. 37, no. 2, pp. 494–505, Apr. 2021.

[19] W. Kim *et al.*, "Bioinspired dual-morphing stretchable origami," *Sci. Robot.*, vol. 4, no. 36, Nov. 2019.

[20] I. L. Delimont, S. P. Magleby, and L. L. Howell, "Evaluating Compliant Hinge Geometries for Origami-Inspired Mechanisms," *J. Mech. Robot.*, vol. 7, no. 1, Feb. 2015.

[21] J. O. Jacobsen, G. Chen, L. L. Howell, and S. P. Magleby, "Lamina Emergent Torsional (LET) Joint," *Mech. Mach. Theory*, vol. 44, no. 11, pp. 2098–2109, Nov. 2009.

[22] J.-E. Suh *et al.*, "Self-Reconfiguring and Stiffening Origami Tube," *Adv. Eng. Mater.*, vol. 24, no. 5, p. 2101202, May 2022.

[23] T. van Manen, S. Janbaz, M. Ganjian, and A. A. Zadpoor, "Kirigami-enabled self-folding origami," *Materials Today*, vol. 32, pp. 59–67, Jan. 2020.

[24] A. Eda *et al.*, "Large Curvature Self-Folding Method of a Thick Metal Layer for Hinged Origami/Kirigami Stretchable Electronic Devices," *Micromachines*, vol. 13, no. 6, p. 907, Jun. 2022.

[25] W. Yan, D. Zhao, and A. Mehta, "Fabrication-aware design for furniture with planar pieces," *Robotica*, vol. 41, no. 1, pp. 48–73, Jan. 2023.

[26] Dongpign Deng and Yong Chen, "Assembled Additive Manufacturing - A Hybrid Farbrication Process Inspired by Origami Design," *2013 Int. Solid Freeform Fabrication Symposium*, 2013.

[27] S.-R. Kim, D.-Y. Lee, S.-J. Ahn, J.-S. Koh, and K.-J. Cho, "Morphing Origami Block for Lightweight Reconfigurable System," *IEEE Trans. Robot.*, vol. 37, no. 2, pp. 494–505, Apr. 2021.

[28] G. E. Maddux, L. A. Vorst, F. J. Giessler, T. Moritz, and TECHNOLOGY INC DAYTON OH, "STRESS ANALYSIS MANUAL," Aug. 1969.

[29] Andrew Pytel and Jaan Kiusalaas, *Mechanics of Materials*, 2nd Edition. Cengage Learning, 2011.

[30] P. Palmieri, M. Melchiorre, and S. Mauro, "Design of a Lightweight and Deployable Soft Robotic Arm," *Robotics*, vol. 11, no. 5, p. 88, Aug. 2022.

[31] S.-J. Kim, D.-Y. Lee, G.-P. Jung, and K.-J. Cho, "An origami-inspired, self-locking robotic arm that can be folded flat," *Sci. Robot.*, vol. 3, no. 16, Mar. 2018.

[32] M. Mahlin, R. L. Wagner, J. Dorsey, and T. C. Jones, "Tendon-Actuated Lightweight In-Space MANipulator (TALISMAN) Hinge Joint Structural," AIAA 2020-4251.ASCEND 2020, Nov. 2020.

[33] S. Liu, F. Wang, Z. Liu, W. Zhang, Y. Tian, and D. Zhang, "A Two-Finger Soft-Robotic Gripper with Enveloping and Pinching Grasping Modes," *IEEE/ASME Trans. Mechatronics*, pp. 1–1, 2020.